High-spin level structure of the semi-magic nucleus ^{91}Nb

P. W. Luo,[1,2] X. G. Wu,[1,*] H. B. Sun,[2,†] G. S. Li,[1] C. Y. He,[1] Y. Zheng,[1] C. B. Li,[1,3] S. P. Hu,[1,2] Y. H. Wu,[1,3] H. W. Li,[1,3] J. J. Liu,[1,2] J. L. Wang,[1] S. H. Yao,[1] and Scott A. Edwards[2]

[1]*China Institute of Atomic Energy, Beijing 102413, China*

[2]*College of Physics Science and Technology, Shenzhen University, Shenzhen 518060, China*

[3]*College of Physics, Jilin University, Changchun 130012, China*

(Received 27 October 2013; revised manuscript received 20 January 2014; published 24 March 2014)

The high-spin level structure of the semi-magic nucleus ^{91}Nb has been investigated via the ^{82}Se(^{14}N,5n)^{91}Nb reaction at a beam energy of 60 MeV. Based on these experimental results, a new level scheme is established that modifies and extends earlier schemes. Shell-model calculations have been carried out to interpret the level structure of ^{91}Nb. The calculated results show that the inclusion of neutron particle-hole excitation across the $N = 50$ shell gap is essential to adequately describe states above $I = (21/2-23/2)\hbar$, with excitation energies above ~6.0 MeV.

DOI: 10.1103/PhysRevC.89.034318 PACS number(s): 23.20.Lv, 25.70.Jj, 21.60.Cs, 27.60.+j

I. INTRODUCTION

As is well known, high angular momentum in nuclei can arise from intrinsic or collective modes of excitation. Intrinsic modes are dominant in nuclei for which the number of protons or neutrons is close to the magic number, whereas collective modes occur in nuclei whose proton and neutron numbers are far away from the closed shell. Nuclei with $N \sim 50$ in the $A \sim 90$ mass region, whose high angular momentum states are due to quasiparticle intrinsic excitations, have attracted considerably theoretical and experimental attention in recent years [1–10]. In particular, investigations of the $N = 50$ isotones in the $A \sim 90$ mass region [10–18] may be of great significance in providing a suitable laboratory for testing the residual interactions of the spherical shell model and to study the mechanism of particle-hole excitations of the $N = 50$ core. Studies of ^{91}Nb isotones have revealed that proton configuration plays a leading role in low-lying states of these semi-magic nuclei, whereas the higher-angular-momentum states are dominated by the excitation of a single $g_{9/2}$ neutron across the $N = 50$ shell closure into the $d_{5/2}$ orbit, similar to ^{88}Sr [11,12], ^{89}Y [13], ^{90}Zr [14], ^{92}Mo [15–17], ^{93}Tc [16–18], ^{94}Ru [10,16–18], and ^{95}Rh [16–18]. However, studies of the higher-angular-momentum states of ^{91}Nb in the framework of a shell model based on experimental data are scant at present. An investigation into the high-spin level structure of ^{91}Nb is therefore essential for improving understanding of the level structures of nuclei with $N \sim 50$ in the $A \sim 90$ mass region.

So far, the high-spin level structure of ^{91}Nb has been investigated via the ^{88}Sr(^{6}Li,3n)^{91}Nb [19], ^{89}Y(α,2n)^{91}Nb [20], and ^{76}Ge(^{19}F,4n)^{91}Nb [21] reactions. The higher-angular-momentum states of ^{91}Nb observed in the present work shown in Fig. 1 are mainly compared with those reported in Ref. [21]. In order to obtain a better understanding of the level structure of ^{91}Nb, shell-model calculations have been performed in two different configuration spaces: $\pi(f_{5/2}, p_{3/2}, p_{1/2}, g_{9/2})\nu(p_{1/2}, g_{9/2})$ (SM-I), and $\pi(f_{5/2}, p_{3/2}, p_{1/2}, g_{9/2})\nu(p_{1/2}, g_{9/2}, d_{5/2})$ (SM-II), relative to a hypothetical ^{66}Ni core.

In this article, new results on the high-spin structure of ^{91}Nb are reported. The experimental details and level scheme of ^{91}Nb are described in Secs. II and III, respectively. Shell-model calculations and discussion of the high-spin structure of ^{91}Nb are presented in detail in Sec. IV. A brief summary is presented in Sec. V.

II. EXPERIMENTAL DETAILS

High-spin states of the semi-magic nucleus ^{91}Nb were populated using the ^{82}Se(^{14}N,5n)^{91}Nb reaction. The ^{14}N beam was delivered by the HI-13 tandem accelerator of the China Institute of Atomic Energy (CIAE) in Beijing. The target consisted of a 0.99 mg/cm^2 layer of ^{82}Se evaporated on an 8.27 mg/cm^2 thick natural Yb backing. The beam energy was selected to be 60 MeV based on the computed results of the statistical evaporation code CASCADE [22] and the experimental excitation function. The detector array was composed of 11 Compton-suppressed hyperpure germanium (HPGe) detectors and two planar type HPGe detectors. In the detector array, detectors were placed at the forward, 90°, and backward directions with respect to the beam direction. Energy and efficiency calibrations were made using the ^{60}Co, ^{133}Ba, and ^{152}Eu standard sources. The typical energy resolution of a Compton-suppressed HPGe detector (or planar type HPGe detector) is 2.0 to 2.5 keV (or 0.6 to 0.7 keV) for the 1332.5 keV (or 121.8 keV) γ ray of ^{60}Co (or ^{152}Eu). A total of about 60 × 10^6 γ-γ coincidence events were collected in event-by-event mode, and the data were sorted into a symmetrized E_γ-E_γ matrix for subsequent offline analysis.

In order to obtain information on the multipolarity of the emitted γ rays, two asymmetric matrices were built, with one axis (y axis) using the γ rays detected at all angles, and the other axis (x axis) using those detected at 40° (or 140°) and those detected at 90°, respectively. From the two matrices, the angular distribution asymmetry (ADO) ratios [23], defined as $R_{ADO}(\gamma) = I_\gamma(40°)/I_\gamma(90°)$, were extracted from the γ-ray coincidence intensities observed by the detectors at either 40°

*wxg@ciae.ac.cn
†hbsun@szu.edu.cn

TABLE I. γ-ray energies, relative intensities, angular distribution asymmetry ratios, and spin-parity assignments of the initial and final states in ^{91}Nb. Uncertainties in intensities are given in parentheses.

E_γ (keV)[a]	I_γ[b]	R_{ADO}	E_i (keV)[c]	E_f (keV)[c]	I_i^π[d]	I_f^π[d]
50.1[g]			2034.0	1983.9	$17/2^-$	$13/2^-$
104.8[g]			104.8	0.0	$1/2^-$	$9/2^+$
185.3	24.5(26)	1.03(12)	6938.5	6753.2	$29/2^{(+)}$	$27/2^{(+)}$
185.5	2.7(4)	0.96(16)	6272.0	6086.5	$(23/2^-)$	$25/2^{(+)}$
186.0[e,f]			6213.9	6027.9	$(23/2^-)$	$(21/2^-)$
193.6[g]			1983.9	1790.3	$13/2^-$	$9/2^-$
232.2[e,f]			6446.1	6213.9	$(25/2^-)$	$(23/2^-)$
254.1	19.1(17)	1.01(5)	4350.1	4096.0	$21/2^{(+)}$	$19/2^{(+)}$
308.6	1.2(3)	0.51(14)	6331.6	6023.0	$25/2^{(+)}$	$23/2^{(+)}$
356.3[g]	84.0(24)	1.65(6)	3465.9	3109.6	$21/2^+$	$17/2^+$
414.6[e,f]	0.6(3)		5956.7	5542.1	$(21/2^-)$	$(21/2^-)$
421.6	21.9(23)	0.68(5)	6753.2	6331.6	$27/2^{(+)}$	$25/2^{(+)}$
429.5[g]			2413.4	1983.9	$11/2^-$	$13/2^-$
449.5	9.4(5)	0.98(5)	3109.6	2660.1	$17/2^+$	$15/2^-$
453.0	3.1(7)	0.58(5)	6409.7	5956.7	$(23/2^-)$	$(21/2^-)$
497.5	16.9(13)	0.75(6)	7436.0	6938.5	$31/2^{(+)}$	$29/2^{(+)}$
531.0[e,f]			8628.9	8097.9		$33/2^{(+)}$
603.5[g]			1790.3	1186.8	$9/2^-$	$5/2^-$
606.9	3.7(5)		6938.5	6331.6	$29/2^{(+)}$	$25/2^{(+)}$
626.1	>9.4	0.95(8)	2660.1	2034.0	$15/2^-$	$17/2^-$
645.2	3.7(10)	0.79(9)	6917.2	6272.0	$(25/2^-)$	$(23/2^-)$
661.9	6.9(5)	0.69(9)	8097.9	7436.0	$33/2^{(+)}$	$31/2^{(+)}$
700.0[e,f]			9328.9	8628.9		
718.0	1.7(4)	0.92(23)	6260.1	5542.1	$(23/2^-)$	$(21/2^-)$
729.9	5.4(6)	0.72(6)	6272.0	5542.1	$(23/2^-)$	$(21/2^-)$
730.2[e]	0.9(2)		6753.2	6023.0	$27/2^{(+)}$	$23/2^{(+)}$
748.0	2.2(3)	0.69(13)	8845.9	8097.9	$35/2^{(+)}$	$33/2^{(+)}$
796.7	1.1(2)	0.85(11)	7713.9	6917.2	$(27/2^-)$	$(25/2^-)$
807.0[e,f]			10135.9	9328.9		
817.4	7.3(20)	1.05(18)	6086.5	5269.1	$25/2^{(+)}$	$23/2^{(+)}$
819.2[g]	74.5(13)	1.64(11)	3109.6	2290.4	$17/2^+$	$13/2^+$
837.5[e]	0.5(2)		7097.6	6260.1	$(25/2^-)$	$(23/2^-)$
867.6[e]	0.8(3)		6409.7	5542.1	$(23/2^-)$	$(21/2^-)$
884.2	29.3(5)	1.34(10)	4350.1	3465.9	$21/2^{(+)}$	$21/2^+$
903.6	9.6(9)	0.72(4)	6086.5	5182.9	$25/2^{(+)}$	$23/2^{(+)}$
919.0	22.8(11)	0.52(5)	5269.1	4350.1	$23/2^{(+)}$	$21/2^{(+)}$
1062.5	8.1(22)	0.55(8)	6331.6	5269.1	$25/2^{(+)}$	$23/2^{(+)}$
1082.0[g]			1186.8	104.8	$5/2^-$	$1/2^-$
1484.1	4.1(1)	1.38(32)	6753.2	5269.1	$27/2^{(+)}$	$23/2^{(+)}$
1717.0	11.0(5)	0.91(9)	5182.9	3465.9	$23/2^{(+)}$	$21/2^+$
1790.3[g]			1790.3	0.0	$9/2^-$	$9/2^+$
1927.0[e]	>2.1		6023.0	4096.0	$23/2^{(+)}$	$19/2^{(+)}$
1981.5	17.8(22)	1.33(18)	6331.6	4350.1	$25/2^{(+)}$	$21/2^{(+)}$
1983.9[g]			1983.9	0.0	$13/2^-$	$9/2^+$
2062.0	25.2(8)	1.02(8)	4096.0	2034.0	$19/2^{(+)}$	$17/2^-$
2076.2	9.2(8)	1.33(14)	5542.1	3465.9	$(21/2^-)$	$21/2^+$
2290.4[g]	100.0(53)		2290.4	0.0	$13/2^+$	$9/2^+$
2490.8	2.6(2)	1.38(31)	5956.7	3465.9	$(21/2^-)$	$21/2^+$
2562.0	1.9(1)		6027.9	3465.9	$(21/2^-)$	$21/2^+$

[a]Uncertainties are between 0.3 and 0.7 keV depending upon their intensity.
[b]Intensities are normalized to the 2290.4 keV transition with $I_\gamma = 100.0$.
[c]Excitation energies of initial E_i and final E_f levels.
[d]Proposed spin and parity assignments to the initial I_i^π and final I_f^π levels.
[e]ADO ratios could not be extracted because of the low intensity of transitions.
[f]Relative intensities could not be determined because of the low intensity of transitions.
[g]The initial- and final-state spins and parities of these transitions are adopted from previous work [19,20].

or 140° and those at 90° by setting gates on the all-angles axis (y axis). For the present geometry, the typical ADO ratio for stretched quadrupole (or $\Delta I = 0$ dipole) transitions was found to be ∼1.4; for stretched pure dipole transitions it was ∼0.8.

III. THE LEVEL SCHEME

The level scheme of ^{91}Nb has been studied previously by Brown *et al.* [19], Fields *et al.* [20], and He *et al.* [21] to excitation energies of 5182, 6009.6, and 10136 keV, respectively. The present level scheme of ^{91}Nb is established on the basis of coincidence relationships, intensity balances, and energy sums. Besides those reported in previous works [19–21], about 14 new γ rays and 7 new levels were observed in this work. The obtained γ-ray energies, relative intensities, angular distribution asymmetry (ADO) ratios, and spin-parity assignments of the initial and final states are listed in Table I. The newly established level scheme of ^{91}Nb, which has been separated into seven groups labeled with letters A through G, is shown in Fig. 1. Typical prompt γ-γ coincidence spectra for ^{91}Nb are shown in Figs. 2–5.

The transitions of the main positive-parity structure in group A with respect to the equivalent structure in Ref. [21] have also been observed in this work. However, the high-spin structure of the transition sequences in this group has been modified based on several newly observed lower-intensity transitions, which will be discussed explicitly in the following.

Spin-parity values of most low-lying states in groups A and B have been firmly determined in Refs. [19,20], as shown in Fig. 1. Spins and parities of the low-lying states between $I^\pi = 9/2^+(G.S)$ and $I^\pi = 21/2^+(E_{\rm exp} = 3465.9$ keV) with a 356.3–819.2–2290.4 keV cascade in group A, have been firmly assigned by Brown *et al.* in previous work [19]. In the coincidence spectrum gated on the 356.3 keV decay (see Fig. 2), the 884.2 keV transition can be seen while the 254.1 and 2062.0 keV transitions do not appear. Therefore, the 254.1–2062.0 keV cascade is placed in parallel with the 356.3 keV transition and the 884.2 keV transition is

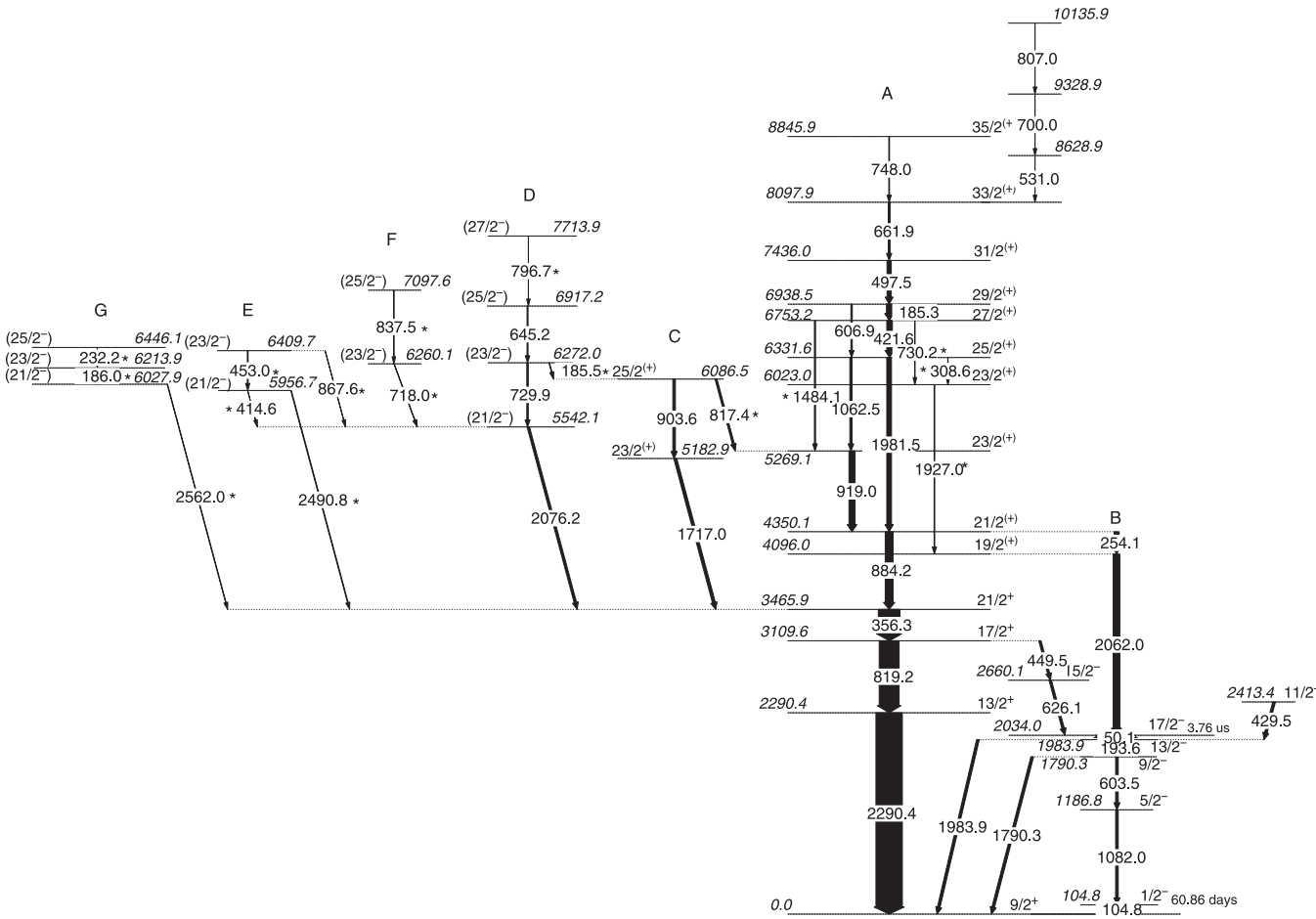

FIG. 1. The level scheme of ^{91}Nb established in the present work. The energies of the γ transitions and of the levels are given in keV. Spins and parities in parentheses are tentative assignments. New γ transitions observed in this work are denoted with asterisks.

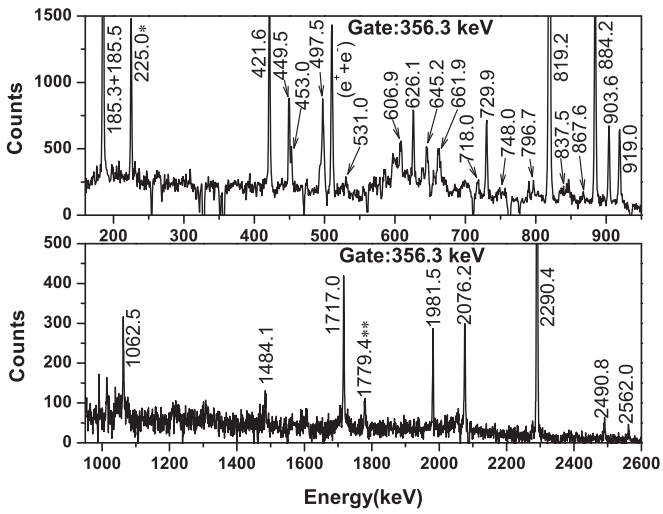

FIG. 2. Background-corrected coincidence spectrum obtained by gating on the 356.3 keV γ ray in group A. The energies with single or double asterisks are contaminations from the reaction channel ^{82}Se(^{14}N,1p3n)^{92}Zr or the single-escape peak of the 2290.4 keV γ ray in ^{91}Nb, respectively.

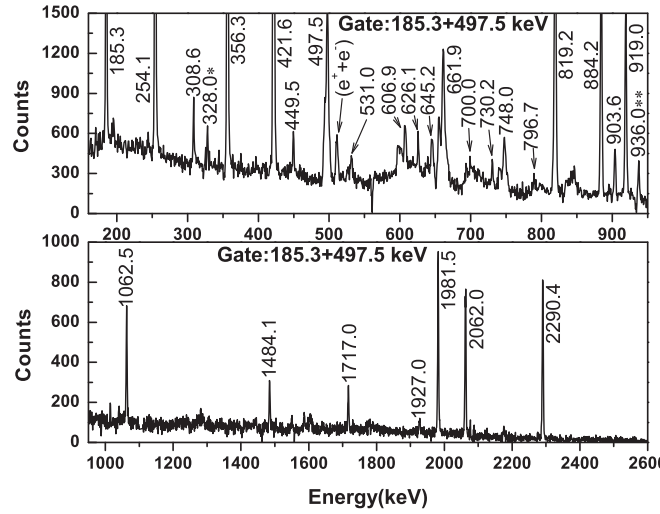

FIG. 3. Background-corrected coincidence spectrum obtained by double gating on the 185.3 and 497.5 keV γ rays in group A. The energies with single or double asterisks are contaminations from the reaction channels ^{82}Se(^{14}N,4n)^{92}Nb or ^{82}Se(^{14}N,3n)^{93}Nb, respectively.

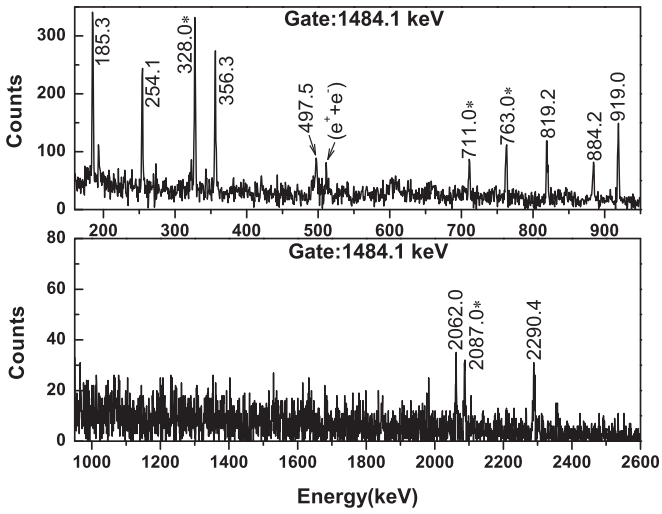

FIG. 4. Background-corrected coincidence spectrum obtained by gating on the 1484.1 keV γ ray in group A. The energies with single asterisk are contaminations from the reaction channel ^{82}Se(^{14}N,4n)^{92}Nb.

placed upon the 3465.9 keV level, which is consistent with that reported in Refs. [19–21]. In addition, the 4350.1 keV level, which was assigned a spin-parity value of $21/2^{(+)}$ in Ref. [20], is given the same spin-parity value of $21/2^{(+)}$ here on the basis of the measured ADO ratio of the 884.2 keV transition. The 919.0, 1062.5, 421.6, 185.3, 1981.5, 606.9, and 497.5 keV transitions, reported in Ref. [21], have also been observed in this work. However, the placement of these transitions has been modified, as shown in Fig. 1, based on the observation of four new lower-intensity transitions: the 308.6, 730.2, 1927.0, and 817.4 keV decays of the 6331.6, 6753.2, 6023.0, and 6086.5 keV levels, respectively. The 919.0, 817.4 (contaminated by 819.2 keV in the 356.3 keV gated spectrum), 1981.5, 1062.5, 606.9, 421.6, 185.3, 497.5, 661.9, and 748.0 keV transitions are displayed in both gated spectra

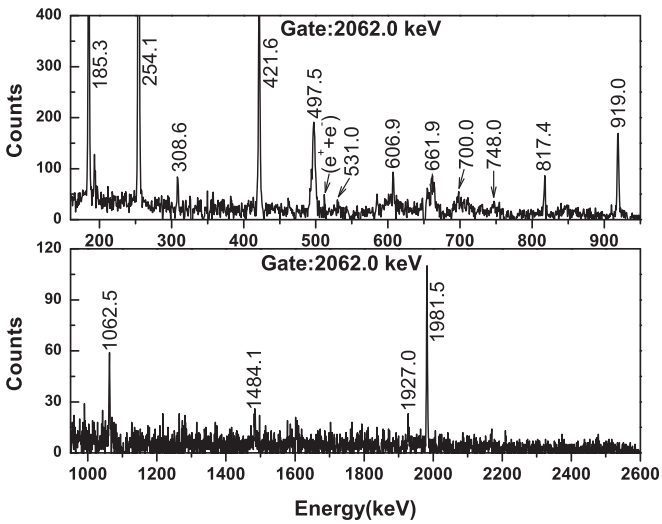

FIG. 5. Background-corrected coincidence spectrum obtained by gating on the 2062.0 keV γ ray in group B.

of the 356.3 and 2062.0 keV γ rays given in Figs. 2 and 5, respectively. However, the 308.6 and 1927.0 keV transitions are only visible in the gated spectrum of the 2062.0 keV γ ray (see Fig. 5). Simultaneously, a new 1484.1 keV crossover transition, which is the sum of the 421.6 and 1062.5 keV transitions, has also been observed. The 1484.1 keV transition can be seen in the gated spectra of the 356.3 (Fig. 2), 497.5–185.3 (Fig. 3), and 2062.0 (Fig. 5) keV γ rays, while the 1062.5, 606.9, 1981.5, and 421.6 keV transitions do not appear in the coincidence spectrum gated on the 1484.1 keV γ ray, as shown Fig. 4. Thus, the 1484.1 keV transition is placed upon the 5269.1 keV level in parallel with the 1062.5, 606.9, 1981.5, and 421.6 keV transitions. The five new transitions have established the reason for modifying the transition sequence in group A with respect to the equivalent structure in Ref. [21].

In addition, ADO ratios extracted for the 919.0, 1062.5, 421.6, 185.3, and 497.5 keV(or 1484.1 and 1981.5 keV) transitions are all consistent with the values expected for $\Delta I = 1$ (or $\Delta I = 2$) transitions, and thereby spins and parities for the 5269.1, 6331.6, 6753.2, 6938.5, and 7436.0 keV levels are proposed to be $23/2^+$, $25/2^+$, $27/2^+$, $29/2^+$, and $31/2^+$, respectively. As for the 6023.0 keV level, a spin value 23/2 is suggested, since the ADO ratio of the 308.6 keV transition has been extracted to be 0.51. The parity of this level is deduced to be positive based on the observation that the 730.2 keV decay of the 6753.2 keV level prefers to have an $E2$ rather than $M2$ character. Accordingly, a spin-parity value of $23/2^+$ is suggested for the 6023.0 keV level. The spin-parity value of the 8845.9 keV level was proposed to be $37/2^+$ in Ref. [21]. However, the multipolarities of the 748.0 and 661.9 keV transitions are assigned to be $\Delta I = 1$ dipole in terms of their measured ADO ratios, and a magnetic character for these two transitions is tentatively proposed. Therefore, the 8097.9 and 8845.9 keV levels are suggested to have spin-parities of $33/2^+$ and $35/2^+$, respectively. The 531.0, 700.0, and 807.0 keV transitions, reported in Ref. [21], have also been observed in our experiment. However, intensities and ADO ratios for these three transitions could not be obtained due to poor data statistics. As a consequence, they are tentatively placed in the order shown in Fig. 1.

The negative-parity states in group B have been reported in Refs. [19,20]. Transitions below the $I^\pi = 17/2^-(E_{\rm exp} = 2034.0$ keV) state, which is an isomer with a half-life of $T_{1/2} = 3.76 \pm 0.12\mu$s [24], are invisible in the gated spectra Figs. 2–5. The $I^\pi = 1/2^-(E_{\rm exp} = 104.8$ keV) state is also an isomer with a half-life $T_{1/2} = 60.86 \pm 0.22$ days [24]. Therefore, spin-parity values of most states in this group are adopted from Ref. [19]. A spin-parity value of $15/2^-$ was made for the 2660.1 keV state in Ref. [20], and we make the same assignment here, since the multipolarities of the 449.5 and 626.1 keV transitions are tentatively assigned as $E1$ and $M1$ types, respectively, based on their measured ADO ratios. With regard to the 4096.0 keV level, a spin-parity value of $(19/2^-)$ and a single spin value of 19/2 were assigned by Brown *et al.* [19] and Fields *et al.* [20], respectively. However, Fields *et al.* were inclined to assign a positive parity for the 4096.0 keV level on the basis of the mixing ratio of the 254.1 keV transition [20]. The measured ADO ratios for the 2062.0 and 254.1 keV transitions have been

extracted to be 1.02 and 1.01, respectively, which are both consistent with the values expected for the $\Delta I = 1$ transitions. Assuming that the $M1$ assignment of the 2062.0 keV decay of the 4096.0 keV level in the previous works [19,21] is correct, the 1927.0 keV $(23/2^{(+)} \rightarrow 19/2^{(-)})$ transition would have an $M2$ character, which would result in a long lifetime of the 6023.0 keV level, and therefore this level would not be observable in this work. Taking the above information into account, we propose an electric character to the 2062.0 keV transition, and the spin-parity value for the 4096.0 keV level is suggested to be $19/2^+$, which is consistent with the theoretical prediction reported by Johnstone *et al.* in Ref. [17] and the shell-model calculations in present work, as shown in Sec. IV.

As for transitions in groups C and D, the 796.7 and 185.5 keV transitions are newly observed. The measured ADO ratios for transitions in the two groups are listed in Table I. Parities of the two groups were proposed to be positive and negative, respectively, in Ref. [21]. We also hold with these parity assignments for the two groups in view of the level structure systematics and the following theoretical considerations. ADO ratios for the 1717.0 and 903.6 keV transitions in group C are extracted to be 0.91 and 0.72, respectively, which indicate that they are characteristic of $\Delta I = 1$ transitions. Thus, the 5182.9 and 6086.5 keV levels are suggested to have spin-parity values of $23/2^+$ and $25/2^+$, respectively, which are supported by the 817.4 keV transition with an $M1$ character decaying from the 6086.5 keV level to feed the 5269.1 keV state. Additionally, the measured ADO ratio for the 2076.2 keV transition has been extracted to be 1.33, and the multipolarity of the 2076.2 keV transition is proposed as a $\Delta I = 0$ dipole with an electric nature. Thus, the spin-parity value for the 5542.1 keV level is assigned to be $(21/2^-)$. ADO ratios extracted for the 729.9, 645.2, and 796.7 keV transitions are all consistent with the values expected for the $M1$ transitions, and therefore spins and parities for the 6272.0, 6917.2, and 7713.9 keV levels are proposed to be $23/2^-$, $25/2^-$, and $27/2^-$, respectively. With respect to the 185.5 keV linking transition, it has been deduced to be an $E1$ transition, which corresponds to its ADO ratio of 0.96.

Transitions in group E are also newly observed in this work. A negative parity is tentatively assigned to this group. On the basis of the coincidence relationships, as well as the ADO ratios of the involved transitions, the spin-parity values for levels in this group are proposed, as shown in Fig. 1. The 2490.8 keV transition, placed upon the 3465.9 keV level in parallel with the 2076.2 keV transition, is suggested to be $\Delta I = 0$ dipole with an electric character based on its measured ADO ratio of 1.38, and therefore the spin-parity value of the 5956.7 keV level is assigned to be $(21/2^-)$. Similarly, the 453.0 keV transition is proposed to be $M1$ in character due to its measured ADO ratio of 0.58, which suggests a spin-parity assignment $23/2^-$ for the 6409.7 keV level.

With respect to the transitions in groups F and G, we are inclined to propose a negative parity for the two groups. As for the 6260.1 keV level in group F, the ADO ratio for the 718.0 keV transition has been extracted to be 0.92, which indicates that the multipolarity of the 718.0 keV transition is of the $M1$ type. As a result, the spin-parity value of the 6260.1 keV level is tentatively assigned to be $23/2^-$. We also suggest that the 837.5 keV transition has an $M1$ character based on the theoretical prediction shown in Table IV, and thus a spin-parity value of $25/2^-$ is proposed for the 7097.6 keV level. On account of the poor data statistics in group G, the ADO ratios of transitions in this group have not been extracted. Since the 2562.0 keV decay of the 6027.9 keV level has been suggested the same multipolarity as that of the 2490.8 keV transition, the spin-parity value for the 6027.9 keV level is tentatively assigned to be $21/2^-$. The 186.0 and 232.2 keV transitions in cascade are both newly observed in this work. However, information on their intensities and multipolarities is unavailable due to the poor data statistics. They are tentatively placed upon the 6027.9 keV level shown in Fig. 1, and spin-parity values of $23/2^-$ and $25/2^-$ are suggested for the 6213.9 and 6446.1 keV levels, respectively.

IV. SHELL-MODEL CALCULATIONS AND DISCUSSION

A. Shell-model calculations

The ^{91}Nb isotones ^{89}Y [13], ^{92}Mo [15–17], ^{93}Tc [16–18], ^{94}Ru [10,16–18], and ^{95}Rh [16–18] have been studied systematically in experiment and theory within the shell-model framework. These studies show that promoting protons from $(f_{5/2}, p_{3/2}, p_{1/2})$ orbits into the $g_{9/2}$ orbit is enough to generate the angular momenta for low-lying states; however, in order to appropriately describe the higher-angular-momentum states observed in our experiment, the excitation of a neutron across the $N = 50$ shell closure is necessary.

In order to interpret the present experimental results, shell-model calculations for ^{91}Nb have been performed. The calculations were carried out in the GWB model space with the residual interaction GWBXG, using the code OXBASH [25]. The GWB model space consists of four proton orbits $\pi(f_{5/2}, p_{3/2}, p_{1/2}, g_{9/2})$ and six neutron orbits $\nu(p_{1/2}, g_{9/2}, g_{7/2}, d_{5/2}, d_{3/2}, s_{1/2})$ relative to an inert ^{66}Ni core. The GWBXG residual interaction combined effective interactions from the bare G matrix of H7B potential [26] with empirically adjusted two-body matrix elements (TBMEs) and single-particle energies (SPEs), since an empirical Hamiltonian for this model space was unavailable. The 974 original TBMEs for this model space were originally taken from the bare G-matrix calculations of Hosaka *et al.* [26]. A number of these calculated TBMEs were then replaced by empirically or experimentally determined values where available. The TBMEs for the $\pi(f_{5/2}, p_{3/2}, p_{1/2}, g_{9/2})$ orbits were replaced with the effective values of Ji and Wildenthal [27]. The TBMEs connecting the $\pi(p_{1/2}, g_{9/2})$ orbits and the $\nu(d_{5/2}, s_{1/2})$ were replaced by those from the work of Gloeckner [28], and those between the $\pi(p_{1/2}, g_{9/2})$ orbits and the $\nu(p_{1/2}, g_{9/2})$ orbits were replaced with those of Serduke *et al.* [29]. In our calculations for ^{91}Nb, the SPEs (in MeV) corresponding to the model space were set as $\epsilon^{\pi}_{f_{5/2}} = -5.322$, $\epsilon^{\pi}_{p_{3/2}} = -6.144$, $\epsilon^{\pi}_{p_{1/2}} = -3.941$, $\epsilon^{\pi}_{g_{9/2}} = -1.250$, $\epsilon^{\nu}_{p_{1/2}} = -0.696$, $\epsilon^{\nu}_{g_{9/2}} = -2.597$, $\epsilon^{\nu}_{g_{7/2}} = +5.159$, $\epsilon^{\nu}_{d_{5/2}} = +1.830$, $\epsilon^{\nu}_{d_{3/2}} = +4.261$, and $\epsilon^{\nu}_{s_{1/2}} = +1.741$. According to the report in Ref. [4], since the proton-proton interactions for the $\pi(f_{5/2}, p_{3/2}, p_{1/2}, g_{9/2})$ orbits were empirically determined by Ji and Wildenthal to describe those nuclei

TABLE II. Truncation was employed by selecting out the dominant configurations to be taken into consideration during our calculations. Each partition is of the form: $P = \pi[p(1), p(2), p(3), p(4)] \otimes \nu[n(1),n(2),n(3),n(4),n(5),n(6)]$, where $p(i)$ represents the number of valence protons occupying the $f_{5/2}$, $p_{3/2}$, $p_{1/2}$, and $g_{9/2}$ orbits, and $n(j)$ represents the number of valence neutrons in the $p_{1/2}$, $g_{9/2}$, $g_{7/2}$, $d_{5/2}$, $d_{3/2}$, and $s_{1/2}$ orbits, respectively. $p(3)$ and $p(4)$ are limited, where $0 \leqslant p(3) \leqslant 2$ and $1 \leqslant p(4) \leqslant 5$, respectively.

Configurations											
Sum of valence protons: 13						Sum of valence neutrons: 12					
$\pi($	$f_{5/2}$,	$p_{3/2}$,	$p_{1/2}$,	$g_{9/2})$	$\otimes$	$\nu(p_{1/2}$,	$g_{9/2}$,	$g_{7/2}$,	$d_{5/2}$,	$d_{3/2}$,	$s_{1/2})$
$\pi($	6,	4,	$p(3)$,	$p(4))$	$\otimes$	$\nu($ 2,	10,	0,	0,	0,	0)
$\pi($	6,	3,	$p(3)$,	$p(4))$	$\otimes$	$\nu($ 2,	10,	0,	0,	0,	0)
$\pi($	6,	2,	$p(3)$,	$p(4))$	$\otimes$	$\nu($ 2,	10,	0,	0,	0,	0)
$\pi($	5,	4,	$p(3)$,	$p(4))$	$\otimes$	$\nu($ 2,	10,	0,	0,	0,	0)
$\pi($	5,	3,	$p(3)$,	$p(4))$	$\otimes$	$\nu($ 2,	10,	0,	0,	0,	0)
$\pi($	5,	2,	$p(3)$,	$p(4))$	$\otimes$	$\nu($ 2,	10,	0,	0,	0,	0)
$\pi($	4,	4,	$p(3)$,	$p(4))$	$\otimes$	$\nu($ 2,	10,	0,	0,	0,	0)
$\pi($	4,	3,	$p(3)$,	$p(4))$	$\otimes$	$\nu($ 2,	10,	0,	0,	0,	0)
$\pi($	4,	2,	$p(3)$,	$p(4))$	$\otimes$	$\nu($ 2,	10,	0,	0,	0,	0)
$\pi($	6,	4,	$p(3)$,	$p(4))$	$\otimes$	$\nu($ 2,	9,	0,	1,	0,	0)
$\pi($	6,	3,	$p(3)$,	$p(4))$	$\otimes$	$\nu($ 2,	9,	0,	1,	0,	0)
$\pi($	6,	2,	$p(3)$,	$p(4))$	$\otimes$	$\nu($ 2,	9,	0,	1,	0,	0)
$\pi($	5,	4,	$p(3)$,	$p(4))$	$\otimes$	$\nu($ 2,	9,	0,	1,	0,	0)
$\pi($	5,	3,	$p(3)$,	$p(4))$	$\otimes$	$\nu($ 2,	9,	0,	1,	0,	0)
$\pi($	5,	2,	$p(3)$,	$p(4))$	$\otimes$	$\nu($ 2,	9,	0,	1,	0,	0)
$\pi($	4,	4,	$p(3)$,	$p(4))$	$\otimes$	$\nu($ 2,	9,	0,	1,	0,	0)
$\pi($	4,	3,	2,	4)	$\otimes$	$\nu($ 2,	9,	0,	1,	0,	0)

with $Z = 32$–46 and $N = 50$ [27], the SPEs of proton orbits were renormalized by taking into consideration the additional proton-neutron interaction between the $\pi(f_{5/2}, p_{3/2}, p_{1/2}, g_{9/2})$ and $\nu(p_{1/2}, g_{9/2})$ orbits, including which the calculations still reproduced the results of Ji and Wildenthal. With respect to the $\nu(g_{7/2}, d_{5/2}, d_{3/2}, s_{1/2})$ orbits, the SPEs were set so as to have a good description of the low-energy spectra in nuclei with $N = 51$ in the $A \sim 90$ mass region, e.g., ^{93}Mo, ^{91}Zr, and ^{89}Sr.

In consideration of the computational difficulties, truncations were employed in our calculation based on the analogous scheme introduced in Ref. [16]. In this truncation scheme, only the dominant configurations for a particular state are taken into consideration, and the results thus obtained differ slightly from the those that would be produced in an unrestricted model space. In order to select out the dominant configurations for a particular state for $N = 50$ isotones in the $A \sim 90$ mass region, the mechanisms for the generation of the observed states should be clarified. On the one hand, for the low-lying states, the valence protons are allowed to move freely among the $\pi(f_{5/2}, p_{3/2}, p_{1/2}, g_{9/2})$ orbits, viz., the valence protons are redistributed in the fpg subspace. Simultaneously, the neutron shells $\nu(p_{1/2}, g_{9/2})$ are kept filled completely. On the other hand, the higher-angular-momentum states are expected to be dominated by the $N = 50$ inert core excitation, namely, a single $\nu g_{9/2}$ neutron across the $N = 50$ shell closure into the $\nu d_{5/2}$ orbit of the next major oscillator shell, which has been observed in ^{92}Mo [15–17], ^{93}Tc [16–18], and in other studies. The configurations of these higher-angular-momentum states are dominated by a neutron particle-hole excitation $\nu(g_{9/2}^{-1}d_{5/2})$ coupled to the valence proton states in fpg subspace. Two configuration spaces, SM-I and SM-II mentioned in Sec. I, were employed in our calculations in consideration of the two mechanisms mentioned above. For the SM-I configuration space, the valence protons were allowed to move freely among the $f_{5/2}$, $p_{3/2}$, $p_{1/2}$, and $g_{9/2}$ orbits, while the $p_{1/2}$ and $g_{9/2}$ neutron orbits were kept full, viz., only the proton excitations were taken into consideration. For the SM-II configuration space, the influence of $\nu(g_{9/2}^{-1}d_{5/2})$ was included, and only the

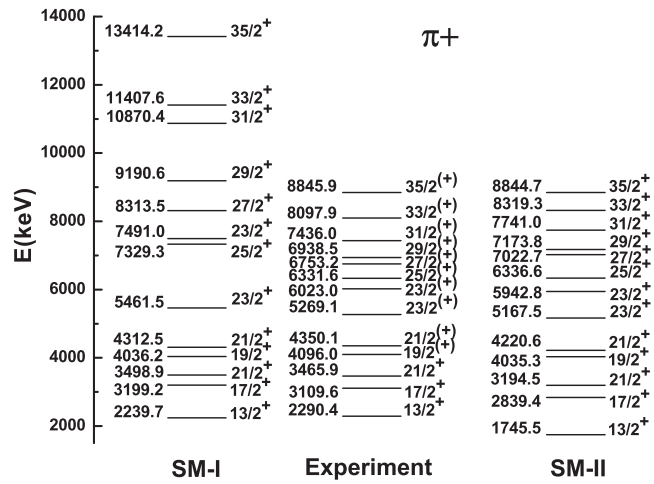

FIG. 6. Comparison of experimental and calculated energy levels of positive-parity yrast states in ^{91}Nb within SM-I and SM-II configuration spaces.

TABLE III. Main partitions of wave functions for ^{91}Nb within the SM-I configuration space. The wave function for a particular angular momentum state would be composed of several partitions. Each partition is of the form $P = \pi[p(1), p(2), p(3), p(4)]$, where $p(i)$ represents the number of valence protons occupying the $f_{5/2}$, $p_{3/2}$, $p_{1/2}$, and $g_{9/2}$ orbits. No neutrons were allowed to be excited to the $d_{5/2}$, $g_{7/2}$, $d_{3/2}$, and $s_{1/2}$ orbits in these calculations.

I^π ($\hbar$)	E_{exp} (keV)	E_{cal} (keV)	Wave function π	Seniority ν	Partitions %
$9/2^+$	0.0	0.0	$\pi(6,4,2,1)$	1	56.1
			$\pi(6,4,0,3)$	1	19.5
			$\pi(6,2,2,3)$	1	14.7
$13/2^+$	2290.4	2239.7	$\pi(6,4,0,3)$	1	51.4
			$\pi(4,4,2,3)$	1	17.2
			$\pi(5,4,1,3)$	3	11.7
$17/2^+$	3109.6	3199.2	$\pi(6,4,0,3)$	1	60.5
			$\pi(4,4,2,3)$	1	13.4
$19/2^{(+)}$	4096.0	4036.2	$\pi(5,4,1,3)$	3	44.1
			$\pi(6,3,1,3)$	3	41.4
$21/2^+$	3465.9	3498.9	$\pi(6,4,0,3)$	1	67.3
			$\pi(4,4,2,3)$	1	10.9
$21/2^{(+)}$	4350.1	4312.5	$\pi(5,4,1,3)$	3	82.8
			$\pi(5,3,2,3)$	3	11.6
$23/2^{(+)}$	5182.9	4834.2	$\pi(5,4,1,3)$	3	81.0
			$\pi(5,3,2,3)$	3	13.9
$23/2^{(+)}$	5269.1	5461.5	$\pi(5,4,1,3)$	3	59.3
			$\pi(5,3,2,3)$	3	28.0
$23/2^{(+)}$	6023.0	7491.0	$\pi(5,3,2,3)$	3	81.8
$25/2^{(+)}$	6086.5	5941.4	$\pi(6,3,1,3)$	3	66.6
			$\pi(4,4,2,3)$	1	11.0
			$\pi(6,2,2,3)$	1	11.0
$25/2^{(+)}$	6331.6	7329.3	$\pi(4,4,0,5)$	1	47.8
			$\pi(4,4,2,3)$	1	27.0
$27/2^{(+)}$	6753.2	8313.5	$\pi(5,3,0,5)$	3	32.0
			$\pi(4,4,0,5)$	1	30.7
			$\pi(4,4,2,3)$	1	13.7
$29/2^{(+)}$	6938.5	9190.6	$\pi(5,3,0,5)$	3	38.5
			$\pi(4,4,2,3)$	1	27.0
			$\pi(5,2,1,5)$	3	14.3
			$\pi(5,3,2,3)$	3	13.8
			$\pi(4,4,2,3)$	1	13.8
			$\pi(4,3,1,5)$	3	13.3
$31/2^{(+)}$	7436.0	10870.4	$\pi(4,3,1,5)$	3	64.3
			$\pi(5,2,1,5)$	3	20.6
$33/2^{(+)}$	8097.9	11407.6	$\pi(4,3,1,5)$	3	63.7
			$\pi(4,2,2,5)$	1	13.6
			$\pi(5,3,0,5)$	3	10.7
$35/2^{(+)}$	8845.9	13414.2	$\pi(4,3,1,5)$	3	36.1
			$\pi(3,4,1,5)$	3	25.5
			$\pi(4,2,2,5)$	1	22.3
$1/2^-$	104.8	202.0	$\pi(6,4,1,2)$	1	83.6
			$\pi(6,2,1,4)$	1	12.9
$5/2^-$	1186.8	1074.4	$\pi(6,4,1,2)$	1	53.9
			$\pi(5,4,2,2)$	1	20.8
$9/2^-$	1790.3	1849.5	$\pi(6,4,1,2)$	1	75.8
$11/2^-$	2413.4	2187.6	$\pi(6,4,1,2)$	1	58.5
			$\pi(6,3,2,2)$	1	26.5
$13/2^-$	1983.9	1962.9	$\pi(6,4,1,2)$	1	73.3
			$\pi(6,3,2,2)$	1	13.8
$15/2^-$	2660.1	2445.0	$\pi(6,4,1,2)$	1	73.6
			$\pi(6,3,2,2)$	1	14.6
$17/2^-$	2034.0	2015.7	$\pi(6,4,1,2)$	1	81.5
$(21/2^-)$	5542.1	5483.0	$\pi(4,4,1,4)$	1	25.4
			$\pi(5,4,0,4)$	1	22.6
			$\pi(6,3,0,4)$	1	15.0
			$\pi(5,3,1,4)$	3	10.5
$(21/2^-)$	5956.7	6649.0	$\pi(5,3,1,4)$	3	50.4
			$\pi(4,4,1,4)$	1	17.9
$(21/2^-)$	6027.9	6740.7	$\pi(5,3,1,4)$	3	61.5
			$\pi(4,4,1,4)$	1	14.9
$(23/2^-)$	6260.1	7187.4	$\pi(5,3,1,4)$	3	59.6
			$\pi(4,4,1,4)$	1	10.1
$(23/2^-)$	6272.0	7378.3	$\pi(5,3,1,4)$	3	41.8
			$\pi(4,4,1,4)$	1	35.1
$(23/2^-)$	6409.7	7651.2	$\pi(5,3,1,4)$	3	34.7
			$\pi(4,4,1,4)$	1	27.9
$(25/2^-)$	6917.2	8258.7	$\pi(5,3,1,4)$	3	44.0
			$\pi(4,4,1,4)$	1	15.2
			$\pi(6,2,1,4)$	1	13.8
$(25/2^-)$	7097.6	7945.4	$\pi(5,3,1,4)$	3	58.8
$(27/2^-)$	7713.9	8660.7	$\pi(5,3,1,4)$	3	61.0
			$\pi(4,3,2,4)$	1	11.9
			$\pi(5,2,2,4)$	1	10.7
			$\pi(4,4,1,4)$	1	10.0

configurations shown in Table II were taken into account in our calculations. The calculated results using these configurations will be discussed in the subsequent section.

B. Discussion

In the present study, the high-spin level structure of ^{91}Nb has been extended and modified compared with that in Refs. [19–21]. The yrast energy levels in ^{91}Nb were studied by Johnstone and Skouras in the shell-model framework allowing $N = 50$ particle-hole excitations [17]. However, ^{91}Nb was not discussed explicitly in Ref. [17] due to the lack of experimental data. Here, we discuss in detail the level structure of ^{91}Nb in the framework of the shell model, based on our new experimental data. The calculated results for positive-parity yrast states in group A within the SM-I and SM-II configuration spaces, as well as the corresponding experimental observations, are shown in Fig. 6. The detailed calculation results are presented in Tables III and IV.

For the positive-parity yrast states in group A, states below $I^\pi = 23/2^{(+)}(E_{exp} = 6023.0\,\text{keV})$ are dominated by the proton states within the $\pi(f_{5/2}, p_{3/2}, p_{1/2}, g_{g/2})$ orbits. The excitation states predicted by these theoretical calculations within the SM-I and SM-II configuration spaces are both in reasonable agreement with those observed in our experiment, with the SM-I predictions being somewhat better that the SM-II. Brown *et al.* [19] and Fields *et al.* [20] predicted that the low-lying states $I^\pi = 13/2^+$, $17/2^+$, and $21/2^+(E_{exp} = 3465.9$ keV) should be dominated by the $\pi(p_{1/2}^{-2} g_{9/2}^3)$ configuration, which

TABLE IV. Main partitions of wave functions for ^{91}Nb within the SM-II configuration space. The wave function for a particular angular momentum state would be composed of several partitions. Each partition is of the form $P = \pi[p(1), p(2), p(3), p(4)] \otimes \nu[n(1),n(2),n(3)]$, where $p(i)$ represents the number of valence protons occupying the $f_{5/2}$, $p_{3/2}$, $p_{1/2}$, and $g_{9/2}$ orbits, and $n(j)$ represents the number of valence neutrons in the $p_{1/2}$, $g_{9/2}$, and $d_{5/2}$ orbits, respectively. No neutrons were allowed to be excited to the $g_{7/2}$, $d_{3/2}$, and $s_{1/2}$ orbits in these calculations.

I^π ($\hbar$)	$E_{\rm exp}$ (keV)	$E_{\rm cal}$ (keV)	Wave function π	Seniority ν	Partitions (%)
$9/2^+$	0.0	0.0	$\pi(6,4,2,1) \otimes \nu(2,10,0)$	1	41.2
			$\pi(6,4,0,3) \otimes \nu(2,10,0)$	1	26.9
			$\pi(6,2,2,3) \otimes \nu(2,10,0)$	1	13.0
$13/2^+$	2290.4	1745.5	$\pi(6,4,0,3) \otimes \nu(2,10,0)$	1	32.2
			$\pi(5,4,1,3) \otimes \nu(2,10,0)$	3	25.2
			$\pi(4,4,2,3) \otimes \nu(2,10,0)$	1	14.9
$17/2^+$	3109.6	2839.4	$\pi(6,4,0,3) \otimes \nu(2,10,0)$	1	50.1
			$\pi(4,4,2,3) \otimes \nu(2,10,0)$	1	15.5
			$\pi(5,4,1,3) \otimes \nu(2,10,0)$	3	10.7
$19/2^{(+)}$	4096.0	4035.3	$\pi(5,4,1,3) \otimes \nu(2,10,0)$	3	51.1
			$\pi(6,3,1,3) \otimes \nu(2,10,0)$	3	28.3
$21/2^+$	3465.9	3194.5	$\pi(6,4,0,3) \otimes \nu(2,10,0)$	1	58.9
			$\pi(4,4,2,3) \otimes \nu(2,10,0)$	1	12.3
$21/2^{(+)}$	4350.1	4220.6	$\pi(5,4,1,3) \otimes \nu(2,10,0)$	3	79.0
$23/2^{(+)}$	5182.9	5167.5	$\pi(5,4,1,3) \otimes \nu(2,10,0)$	3	53.3
			$\pi(5,3,2,3) \otimes \nu(2,10,0)$	3	19.5
$23/2^{(+)}$	5269.1	5544.0	$\pi(5,4,1,3) \otimes \nu(2,10,0)$	3	51.8
			$\pi(6,3,1,3) \otimes \nu(2,10,0)$	3	23.9
			$\pi(5,3,2,3) \otimes \nu(2,10,0)$	3	12.1
$23/2^{(+)}$	6023.0	5942.8	$\pi(5,4,1,3) \otimes \nu(2,9,1)$	5	25.0
			$\pi(6,4,0,3) \otimes \nu(2,9,1)$	3	21.9
			$\pi(4,4,2,3) \otimes \nu(2,9,1)$	3	18.0
$25/2^{(+)}$	6086.5	5838.8	$\pi(6,3,1,3) \otimes \nu(2,10,0)$	3	57.7
			$\pi(5,3,2,3) \otimes \nu(2,10,0)$	3	12.3
$25/2^{(+)}$	6331.6	6336.6	$\pi(6,4,0,3) \otimes \nu(2,9,1)$	3	29.1
			$\pi(5,4,1,3) \otimes \nu(2,9,1)$	5	27.2
			$\pi(4,4,2,3) \otimes \nu(2,9,1)$	3	22.3
$27/2^{(+)}$	6753.2	7022.7	$\pi(5,4,1,3) \otimes \nu(2,9,1)$	5	34.3
			$\pi(6,4,0,3) \otimes \nu(2,9,1)$	3	26.2
			$\pi(4,4,2,3) \otimes \nu(2,9,1)$	3	16.1
$29/2^{(+)}$	6938.5	7173.8	$\pi(6,4,0,3) \otimes \nu(2,9,1)$	3	44.9
			$\pi(4,4,2,3) \otimes \nu(2,9,1)$	3	19.3
			$\pi(5,4,1,3) \otimes \nu(2,9,1)$	5	12.7
$31/2^{(+)}$	7436.0	7741.0	$\pi(6,4,0,3) \otimes \nu(2,9,1)$	3	44.8
			$\pi(4,4,2,3) \otimes \nu(2,9,1)$	3	17.4
			$\pi(5,4,1,3) \otimes \nu(2,9,1)$	5	13.6
			$\pi(6,3,1,3) \otimes \nu(2,9,1)$	5	10.5
$33/2^{(+)}$	8097.9	8319.3	$\pi(5,4,1,3) \otimes \nu(2,9,1)$	5	76.3
			$\pi(5,3,2,3) \otimes \nu(2,9,1)$	5	19.3
$35/2^{(+)}$	8845.9	8844.7	$\pi(5,4,1,3) \otimes \nu(2,9,1)$	5	80.0
			$\pi(5,3,2,3) \otimes \nu(2,9,1)$	5	14.7
$1/2^-$	104.8	129.3	$\pi(6,4,1,2) \otimes \nu(2,10,0)$	1	79.5
			$\pi(6,2,1,4) \otimes \nu(2,10,0)$	1	11.1
$5/2^-$	1186.8	962.8	$\pi(6,4,1,2) \otimes \nu(2,10,0)$	1	57.8
			$\pi(5,4,2,2) \otimes \nu(2,10,0)$	1	19.1
$9/2^-$	1790.3	1774.4	$\pi(6,4,1,2) \otimes \nu(2,10,0)$	1	71.2
			$\pi(5,4,2,2) \otimes \nu(2,10,0)$	1	10.4
$11/2^-$	2413.4	2264.9	$\pi(6,4,1,2) \otimes \nu(2,10,0)$	1	62.2
			$\pi(6,3,2,2) \otimes \nu(2,10,0)$	1	20.8
$13/2^-$	1983.9	1993.4	$\pi(6,4,1,2) \otimes \nu(2,10,0)$	1	77.5
$15/2^-$	2660.1	2435.5	$\pi(6,4,1,2) \otimes \nu(2,10,0)$	1	70.5
			$\pi(6,3,2,2) \otimes \nu(2,10,0)$	1	13.9
$17/2^-$	2034.0	2030.6	$\pi(6,4,1,2) \otimes \nu(2,10,0)$	1	79.1

TABLE IV. *(Continued.)*

I^π ($\hbar$)	$E_{\rm exp}$ (keV)	$E_{\rm cal}$ (keV)	Wave function π	Seniority ν	Partitions (%)
$(21/2^-)$	5542.1	5524.7	$\pi(5,4,0,4)\otimes\nu(2,10,0)$	1	31.3
			$\pi(4,4,1,4)\otimes\nu(2,10,0)$	1	16.1
			$\pi(6,3,0,4)\otimes\nu(2,10,0)$	1	15.7
			$\pi(5,3,1,4)\otimes\nu(2,10,0)$	3	13.1
$(21/2^-)$	5956.7	6213.1	$\pi(6,4,1,2)\otimes\nu(2,9,1)$	3	62.5
			$\pi(5,4,2,2)\otimes\nu(2,9,1)$	3	16.1
			$\pi(6,3,2,2)\otimes\nu(2,9,1)$	3	10.8
$(21/2^-)$	6027.9	6225.8	$\pi(6,4,1,2)\otimes\nu(2,9,1)$	3	63.1
			$\pi(6,3,2,2)\otimes\nu(2,9,1)$	3	14.5
			$\pi(5,4,2,2)\otimes\nu(2,9,1)$	3	12.4
$(23/2^-)$	6260.1	6492.4	$\pi(6,4,1,2)\otimes\nu(2,9,1)$	3	73.0
			$\pi(5,4,2,2)\otimes\nu(2,9,1)$	3	13.1
$(23/2^-)$	6272.0	6208.5	$\pi(6,4,1,2)\otimes\nu(2,9,1)$	3	69.2
			$\pi(6,3,2,2)\otimes\nu(2,9,1)$	3	19.8
$(23/2^-)$	6409.7	6612.8	$\pi(6,4,1,2)\otimes\nu(2,9,1)$	3	59.7
			$\pi(5,4,2,2)\otimes\nu(2,9,1)$	3	20.6
$(25/2^-)$	7097.6	6891.8	$\pi(5,4,2,2)\otimes\nu(2,9,1)$	3	44.4
			$\pi(6,4,1,2)\otimes\nu(2,9,1)$	3	30.8
$(25/2^-)$	6917.2	7262.6	$\pi(6,4,1,2)\otimes\nu(2,9,1)$	3	59.7
			$\pi(6,3,2,2)\otimes\nu(2,9,1)$	3	14.4
			$\pi(5,4,2,2)\otimes\nu(2,9,1)$	3	13.7
$(27/2^-)$	7713.9	7812.2	$\pi(6,4,1,2)\otimes\nu(2,9,1)$	3	38.4
			$\pi(5,4,2,2)\otimes\nu(2,9,1)$	3	24.6
			$\pi(5,4,0,4)\otimes\nu(2,9,1)$	3	14.6

is consistent with the theoretical predictions in our calculations. The low-lying states can also be well described by weak coupling between a $g_{9/2}$ valence proton and the $^{90}_{40}$Zr core [21]. The $I^\pi = 19/2^{(+)}(E_{\rm exp} = 4096.0\,{\rm keV})$, $I^\pi = 21/2^{(+)}(E_{\rm exp} = 4350.1\,{\rm keV})$, and $I^\pi = 23/2^{(+)}(E_{\rm exp} = 5269.1\,{\rm keV})$ states, reproduced within the SM-I and SM-II configuration spaces with deviations of less than 300.0 keV, are found to be dominated by the $\pi(f_{5/2}^{-1}p_{1/2}^{-1}g_{9/2}^{3})$ configuration. However, for the states above $I^\pi = 23/2^{(+)}(E_{\rm exp} = 5269.1\,{\rm keV})$, the predicted values for the excitation energies calculated within the two different configuration spaces (SM-I and SM-II) diverge markedly. As the calculated results show in Fig. 6 (see Tables III and IV for details), the level energies of these states can be reproduced well within the SM-II configuration space; the maximum deviation between the experimental observation and the theoretical prediction above the $I^\pi = 23/2^{(+)}(E_{\rm exp} = 5269.1\,{\rm keV})$ state is just 305.0 keV for the $I^\pi = 31/2^{(+)}(E_{\rm exp} = 7436.0\,{\rm keV})$ state, whereas using the SM-I configuration space leads to a discrepancy of more than 1.0 MeV. Furthermore, the discrepancy increases as the angular momentum increases, in general.

It is well known that the phenomenon of the breaking of the $N = 50$ core is universal in the ^{91}Nb isotones, as has been mentioned in Sec. I. Generally, the excitation of a neutron in the $g_{9/2}$ orbit across the $N = 50$ shell gap into the $d_{5/2}$ orbit is of great significance in describing the higher-angular-momentum states of these semi-magic nuclei. With respect to the nucleus ^{91}Nb, the same phenomenon should also be observed in its higher-angular-momentum states. As shown in Table IV, the positive-parity yrast states above $I^\pi = 23/2^{(+)}(E_{\rm exp} = 5269.1\,{\rm keV})$ are dominated by the particle-hole excitation of the $N = 50$ inert neutron core, viz., a neutron in the $g_{9/2}$ orbit crossing the $N = 50$ major shell gap coupled to the valence protons states in the fpg subspace. The breaking of the $N = 50$ neutron core is indicated by the presence of 1981.5 and 1927.0 keV transitions decaying from the $I^\pi = 25/2^{(+)}(E_{\rm exp} = 6331.6\,{\rm keV})$ and $I^\pi = 23/2^{(+)}(E_{\rm exp} = 6023.0\,{\rm keV})$ states to the $I^\pi = 21/2^{(+)}(E_{\rm exp} = 4350.1\,{\rm keV})$ and $I^\pi = 19/2^{(+)}(E_{\rm exp} = 4096.0\,{\rm keV})$ states, respectively. States in the range $23/2^{(+)}(E_{\rm exp} = 6023.0\,{\rm keV}) \leqslant I^\pi \leqslant 31/2^{(+)}(E_{\rm exp} = 7436.0\,{\rm keV})$ have significant contributions from a neutron particle-hole excitation $\nu(g_{9/2}^{-1}d_{5/2})$ coupled to the five-quasiparticle proton states in the fpg subspace, as shown in Table IV. States $I^\pi = 33/2^{(+)}(E_{\rm exp} = 8097.9\,{\rm keV})$ and $I^\pi = 35/2^{(+)}(E_{\rm exp} = 8845.9\,{\rm keV})$ are dominated by the $\pi(f_{5/2}^{-1}p_{1/2}^{-1}g_{9/2}^{3})\otimes\nu(g_{9/2}^{-1}d_{5/2})$ configuration based on the shell-model predictions. In addition, we find that a cascade depopulates the $I^\pi = 35/2^{(+)}(E_{\rm exp} = 8845.9\,{\rm keV})$ state via several fast $M1$ transitions including the 748.0, 661.9, and 497.5 keV lines, which is in accord with the properties of the level structures of the $N = 50$ particle-hole excitation in the $A \sim 90$ mass region, since the participation of a $g_{9/2}$ proton particle and a $g_{9/2}$ neutron hole often leads to the enhancement of the magnetic moments [30].

In general, the extent of the deviation between an experimental observation and the corresponding theoretical prediction depends on the contribution of the neglected configurations to the wave function of the state. Omission of a dominant configuration would result in the predicted excitation energy being considerably higher than the experimental

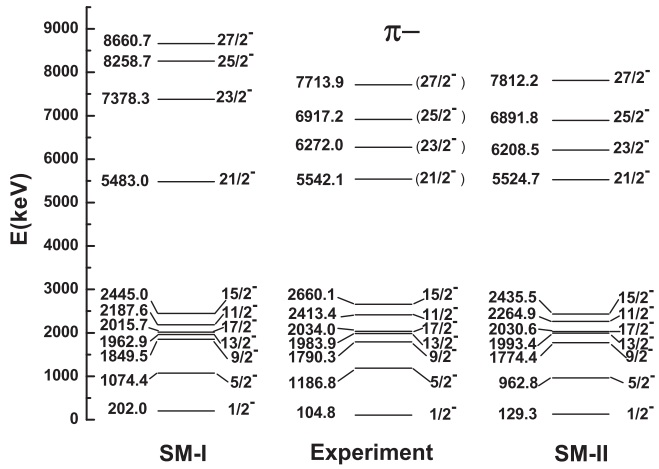

FIG. 7. Comparison of experimental and calculated energy levels of negative-parity non-yrast states in groups B and D of ^{91}Nb within SM-I and SM-II configuration spaces.

one [16]. Thus the reason for the considerable disagreements between the experimental observations and the theoretical predictions for states above $I^\pi = 23/2^{(+)}(E_{\rm exp} = 5269.1\,{\rm keV})$ within the SM-I configuration space is probably that the SM-I configuration space, which excludes the particle-hole excitation of $N = 50$ core, is not large enough to accurately describe all the observed states of ^{91}Nb.

For the negative-parity non-yrast states in groups B and D, the experimental excitation energies and theoretical predictions are compared in Fig. 7, and a detailed comparison is given in Tables III and IV. On the one hand, the states below $I^\pi = (23/2^-)(E_{\rm exp} = 6272.0\,{\rm keV})$ are dominated by the excitation of protons from $(f_{5/2}, p_{3/2}, p_{1/2})$ orbits to the $g_{9/2}$ orbit in the fpg subspace. According to the theoretical predictions, states from $I^\pi = 1/2^-$ at 104.8 keV to $I^\pi = 17/2^-$ at 2034.0 keV have the dominant configuration of $\pi(p_{1/2}^{-1}g_{9/2}^2)$, which is consistent with that reported in Ref. [19,20]. For the $I^\pi = (21/2^-)(E_{\rm exp} = 5542.1\,{\rm keV})$ state, the agreement between the theory and the experiment is also quite good in both configuration spaces. In terms of the theoretical prediction, the configurations of the $I^\pi = (21/2^-)(E_{\rm exp} = 5542.1\,{\rm keV})$ state are also suggested to be dominated by the excitation of protons from $(f_{5/2}, p_{3/2}, p_{1/2})$ orbits into the $g_{9/2}$ orbit. On the other hand, the dominant predicted configurations for states above $I^\pi = (21/2^-)(E_{\rm exp} = 5542.1\,{\rm keV})$ differ greatly depending on which of the SM-I or the SM-II configuration spaces is used. The theoretical predictions within the SM-II configuration space are in good agreement with the experimental results, while the results using the SM-I configuration space are in strong disagreement with experiment, with discrepancies as large as 1.0 MeV. The probable reason is that the contributions from particle-hole excitation in the $N = 50$ inert core have not been taken into consideration, as mentioned earlier. The theoretical predictions within the SM-II configuration space, shown in Table IV, confirm this suspicion: according to the SM-II results, the configurations of states above $I^\pi = (21/2^-)(E_{\rm exp} = 5542.1\,{\rm keV})$ are dominated by configurations involving $\nu(g_{9/2}^{-1}d_{5/2})$ core excitation.

For the positive-parity non-yrast states in group C, the $I^\pi = 23/2^{(+)}(E_{\rm exp} = 5182.9\,{\rm keV})$ and $I^\pi = 25/2^{(+)}(E_{\rm exp} = 6086.5\,{\rm keV})$ states are both dominated by the redistribution of the valence protons in the fpg subspace. The assignments are consistent with those reported in Ref. [21].

As for the states in groups E, F, and G, they also have great contributions from the particle-hole excitation of the $N = 50$ inert core, which is indicated by the presence of transitions with high energy—about 2.5 MeV—depopulating the states with excitation energy ∼6.0 MeV.

V. SUMMARY

The high-spin states of ^{91}Nb have been investigated via the ^{82}Se(^{14}N,5n)^{91}Nb reaction at a beam energy of 60 MeV. The level scheme of ^{91}Nb has been modified and extended. About fourteen new γ rays and seven new levels have been added to the scheme of ^{91}Nb.

Large-basis shell model calculations have been performed to interpret the experimental level scheme of ^{91}Nb. The states below $I = (21/2-23/2)\hbar$ with excitation energy below ∼5.6 MeV can be well described by the redistribution of valence protons in fpg subspace. However, the properties of positive- and negative-parity states above $I = (21/2-23/2)\hbar$ with excitation energies above ∼6.0 MeV can be attributed to the neutron-particle-hole excitation of the $N = 50$ inert core—specifically, the excitation of a single $g_{9/2}$ neutron across the $N = 50$ shell closure into the $d_{5/2}$ orbits coupled to the valence proton states in the fpg valence space.

ACKNOWLEDGMENTS

We would like to thank the crew of the HI-13 tandem accelerator at the China Institute of Atomic Energy for steady operation of the accelerator. We are also grateful to Dr. Q. W. Fan for assistance during target preparation, and appreciate Prof. B. A. Brown at Michigan State University for his OXBASH code. This work is partially supported by the National Natural Science Foundation of China under Grants No. 10927507, No. 11075214, No. 10675171, No. 11175259, and No. 10775098.

[1] X. Z. Cui *et al.*, Phys. Rev. C **72**, 044322 (2005).
[2] A. Chakraborty *et al.*, Phys. Rev. C **72**, 054309 (2005).
[3] T. Fukuchi *et al.*, Eur. Phys. J. A **24**, 249 (2005).
[4] D. Bucurescu *et al.*, Phys. Rev. C **71**, 034315 (2005).
[5] D. Bucurescu *et al.*, Phys. Rev. C **76**, 064301 (2007).
[6] Y. Wakabayashi *et al.*, J. Phys. Soc. Jpn. **76**, 114202 (2007).
[7] C. J. Xu *et al.*, Phys. Rev. C **86**, 027302 (2012).
[8] S. Saha *et al.*, Phys. Rev. C **86**, 034315 (2012).
[9] M. Bunce *et al.*, Phys. Rev. C **87**, 044337 (2013).
[10] F. Ghazi Moradi *et al.*, Phys. Rev. C **89**, 014301 (2014).
[11] E. A. Stefanova *et al.*, Nucl. Phys. A **669**, 14 (2000).
[12] E. A. Stefanova *et al.*, Phys. Rev. C **62**, 054314 (2000).
[13] J. Reif, G. Winter, R. Schwengner, H. Prade, and L. Käubler, Nucl. Phys. A **587**, 449 (1995).

[14] E. K. Warburton, J. W. Olness, C. J. Lister, R. W. Zurmühle, and J. A. Becker, Phys. Rev. C **31**, 1184 (1985).
[15] N. S. Pattabiraman *et al*., Phys. Rev. C **65**, 044324 (2002).
[16] S. S. Ghugre and S. K. Datta, Phys. Rev. C **52**, 1881 (1995).
[17] I. P. Johnstone and L. D. Skouras, Phys. Rev. C **55**, 1227 (1997).
[18] H. A. Roth *et al*., Phys. Rev. C **50**, 1330 (1994).
[19] B. A. Brown, P. M. S. Lesser, and D. B. Fossan, Phys. Rev. C **13**, 1900 (1976).
[20] C. A. Fields, J. J. Kraushaar, R. A. Ristinen, and L. E. Samuelson, Nucl. Phys. A **326**, 55 (1979).
[21] C.-Y. He *et al*., Chin. Phys. Lett. **27**, 102104 (2010).
[22] F. Pühlhofer, Nucl. Phys. A **280**, 267 (1977).
[23] M. Piiparinen *et al*., Nucl. Phys. A **605**, 191 (1996).
[24] Coral M. Baglin, Nucl. Data. Sheets **86**, 1 (1999).
[25] B. A. Brown, A. Etchegoyen, N. S. Godwin *et al*., MSU-NSCL Report number 1289 (unpublished).
[26] A. Hosaka, K.-I. Kubo, and H. Toki, Nucl. Phys. A **444**, 76 (1985).
[27] X. Ji and B. H. Wildenthal, Phys. Rev. C **37**, 1256 (1988).
[28] D. H. Gloeckner, Nucl. Phys. A **253**, 301 (1975).
[29] F. J. D. Serduke, R. D. Lawson, and D. H. Gloeckner, Nucl. Phys. A **256**, 45 (1976).
[30] L. Funke *et al*., Nucl. Phys. A **541**, 241 (1992).